Multilayer Half-Mode Substrate Integrated Waveguide Wideband Coupler with High Selectivity

Zhigang Zhang, Yong Fan, and Yonghong Zhang

Fundamental Science on Extreme High Frequency Key Laboratory
University of Electronic Science and Technology of China, Chengdu 611731, China
freemanzzg@163.com, yfan@uestc.edu.cn, zhangyhh@uestc.edu.cn

Abstract ─ A novel 3dB wideband coupler with enhanced selectivity has been proposed and developed in multilayer HMSIW topology. Periodic ginkgo leaf slots (GLS) are etched on top layer of HMSIW to realize a pass-band combining with high-pass characteristics of HMSIW. The novel GLS cells have stop-band characteristics aiming to improve the frequency selectivity and extend the upper stop-band. Moreover, the roll-off at the upper side is very sharper. A continuous coupling slot is etched in the conductor layer at the broadwall of HMSIW. Coupling takes place through the long, offset slot, which features a flexible design providing a wide coupling dynamic range with wideband characteristics. Detailed design process is introduced to synthesize a wideband filtering HMSIW coupler with better stop-band rejection. The novel coupler is showing a 34.9% coupling bandwidth at 8.87 GHz with good isolation, reflection and out-of-band rejection performances. Its stop band is from 13.8 to 17.6GHz with the rejection more than 40dB. Good agreement is obtained between the simulated and measured results of the proposed structure.

Index Terms ─ Electromagnetic band gap (EBG), Half-mode Substrate Integrated Waveguide (HMSIW), high selectivity, multilayer, wideband coupler.

I. INTRODUCTION

Directional couplers are essential components in transceivers for microwave communication systems. Because they have a great impact on the overall system performance, wideband, low insertion losses and high isolation are usually required in many applications. The substrate integrated waveguide (SIW) technology [1-17] is a promising candidate for modern wireless transceiver systems and has provided an excellent trade-off between waveguide and planar technologies [18-24] in terms of quality factor, volume, the losses, power handling and easy integration.

Nevertheless, the conventional SIW circuits are still too large for millimeter wave systems. Several solutions have been proposed to reduce the footprint of SIW structures, including the half-mode substrate integrated waveguide (HMSIW) [2-6] and the substrate integrated folded waveguide (SIFW) [7-8]. These two topologies allow the width of the SIW to be reduced by a factor of two. In [2], a 3-dB coupler is realized at Ku band using HMSIW, which keeps the good performance of the SIW coupler with nearly a half reduction in size. A ridged HMSIW was proposed in [5], which open side is capacitively loaded with a continuous ridge so as to lower the first-mode cutoff frequency. In [8], the proposed dual-band rat-race coupler was developed in the FSIW, consisting of two stacked layers of substrates.

Recently, miniaturization design is becoming one of the primary trends for many applications in transceivers. On one hand, the use of multilayered topologies [9-11] is known to provide more freedom to design coupling paths and control coupling levels between waveguided structures while preserving a compact circuit size. On the other hand, more and more attention has been paid to single devices integrated with different functionalities, such as a bandpass balun, bandpass coupler [12], and bandpass antenna [13]. A reduced size rat-race SIW coupler incorporating a bandpass frequency response characteristic was presented in [12].

The SIW has highpass performance and the periodic electromagnetic band gap (EBG) structures have slow-wave and stop-band characteristics [14-16]. As such, a periodic configuration is etched on the top layers of the HMSIW to realize the wideband filtering response. In [14], an EBG-loaded ridge substrate integrated waveguide (RSIW) ring coupler was presented. The periodic EBG structures are employed to increase the propagation constant to achieve further size reduction. In [16], a wideband directional coupler was proposed on the basis of the concept of slow-wave HMSIW to achieve compact size. Generally speaking, some problems faced by the above-mentioned structures are poor stopband suppression or narrower bandwidth. How to solve these two problems at the same time has been attracting increasing attention.

In this paper, to overcome the limitation of a conventional coupler, a novel wideband directional

Submitted On: November 19, 2018
Accepted On: March 3, 2019

filtering coupler with enhanced selectivity has been proposed and developed in multilayer HMSIW topology. Periodic ginkgo leaf slots (GLS) are etched on top layer of HMSIW to realize a pass-band combining with high-pass characteristics of HMSIW. The dimensions of the coupling slot and HMSIW are used to determine both the coupling ratio and the center frequency. Meanwhile, it is possible to control the bandwidth and the rejection level by adjusting the parameters of GLS. It's a good combination of multilayered topologies, HMSIW and EBG structures.

II. ANALYSIS AND DESIGN

A. Filtering coupler structure

As shown in Fig. 1 (a), Port 1 is the input port; Port 2 is the through port, whereas Ports 3 and 4 are coupling port and isolation port, respectively.

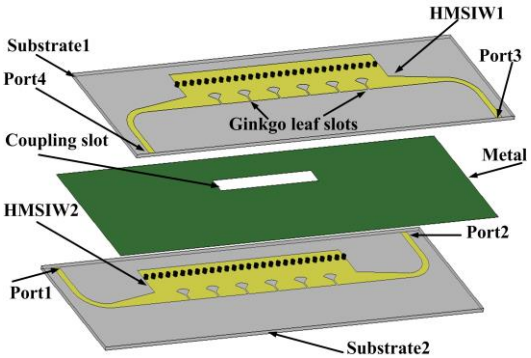

(a)

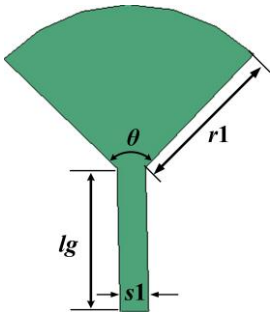

(b)

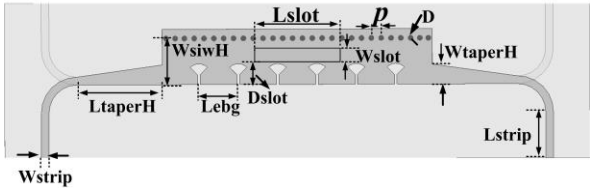

(c)

Fig. 1. The proposed HMSIW filtering coupler with GLS cells: (a) anatomy view, (b) geometries of ginkgo leaf slots (GLS), and (c) top view.

The multilayer E-plane HMSIW coupler consists of two parallel waveguides (HMSIW1 and 2) coupled together by means of a longitudinal slot etched in their common broad wall. The long coupling slot have variable lengths (Lslot), widths(Wslot) and offsets (Dslot), and are arranged with respect to the distribution of $TE_{0.5,0}$ mode. In the coupling region, the coupling slot is located on the metal plane between substrate 1 and 2. As depicted in Fig. 1 (b) and Fig. 1 (c), a periodic GLS configuration is etched on the top layer of the HMSIW1 and 2 to realize the wideband filtering response.

B. Analysis of coupler

As discussed above, the width of the HMSIW is half that of the SIW, so the width of an SIW properly operating in the same frequency range should be determined at first on the basis of the design considerations in [2-3]. The HMSIW has highpass performance and the electromagnetic band gap (EBG) structures have stop-band characteristics.

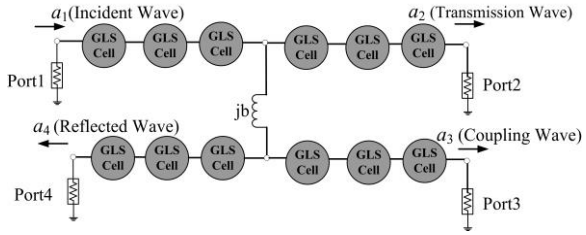

Fig. 2. Schematic of the filtering coupler with GLS.

Figure 2 illustrates the schematic of a four-port filtering coupler. As seen, the proposed structure integrates a bandpass filter and a directional coupler. There are three steps to design the proposed coupler. First, the cutoff frequency for the HMSIW can be determined by the following formulae:

$$a_{eff} = a_{siw} - \frac{D^2}{0.95 \cdot p}, \quad f_{c(TE10)} = \frac{c}{2a_{eff}\sqrt{\varepsilon_r}}. \tag{1}$$

Where, a_{eff} and a_{siw} are the equivalent and real width of SIW, respectively. a_{Hsiw} is the width of HMSIW (a_{siw}=2a_{Hsiw}). D and p are the diameter of metallized via-holes and center-to-center pitch between two adjacent via-holes. c is the light velocity in vacuum, and ε_{r} is the dielectric constant of substrate. Secondly, the dimensions of the coupling slot and the feed lines for transition between the HMSIW and the microstrip are determined to achieve equal coupling strength. Finally, the parameters of the GLS and the periodic separation can be determined by using electromagnetic simulation to obtain good out-of-band rejection.

As observed in Fig. 1 (a) and Fig. 3, the physical fields existing in the structure can always be expressed as the superposition of these two modes, i.e. even mode

and odd mode. When the ports 1 and 4 are excited with two signals of same amplitude and phase, only $TE_{0.5,\,0}$ mode (even mode) can be observed in the coupling region. However, when the two ports are excited by two signals with same amplitude but reverse phase, only TEM mode (odd mode) can be found. The electric field intensities of $TE_{0.5,\,0}$ mode and TEM mode are summed at ports 2 and 3, resulting in the power output at these two ports.

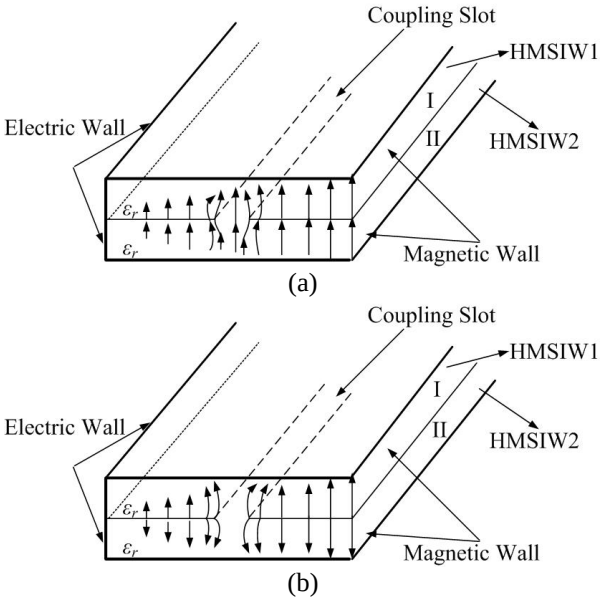

Fig. 3. Electric field distribution in coupling region: (a) even mode and (b) odd mode.

The superposition filed in the coupling slot satisfies [10]:

$$A_I(z) = a_1 e^{-j\beta z}\cos(Kz), \tag{2}$$

$$A_{II}(z) = j a_1 e^{-j\beta z}\sin(Kz), \tag{3}$$

$$K = \frac{1}{2}(\beta_e - \beta_o) = \frac{1}{2}\Delta\beta = \pi(1/\lambda_{0.5,0} - 1/\lambda_{TEM}), \tag{4}$$

where, β_e and β_o are the propagation constant of even mode and odd mode respectively. In this way, within the coupling region, there are two kinds of modes, namely $TE_{0.5,\,0}$ mode in HMSIW and *TEM* mode in stripline. Supposing the length of the coupling region as *L*, the wavelength of $TE_{0.5,\,0}$ mode in HMSIW as $\lambda_{0.5,0}$, whereas the wavelength of *TEM* mode as λ_{TEM}. The coupling ratio at port 3 can be controlled by changing the size of the coupling region, it can be defined as:

$$C = 20\times\lg\left|\frac{A_{II}(L)}{a_1}\right| = 20\times\lg\left|\sin(KL)\right| = 20\times\lg\left|\sin(\frac{\Delta\beta}{2}L)\right|. \tag{5}$$

For a 3-dB coupler(*C*=-3dB), we have,

$$\Delta\beta L = \pi/2 = (\beta_e - \beta_o)\,L. \tag{6}$$

According to reflection suppression condition of $TE_{0.5,\,0}$ mode at both ends of coupling region [25]:

$$1 + e^{-j2\beta_e L} = 0. \tag{7}$$

Based on (7), we have,

$$\sin(2\beta_e L)=0, \text{ and } \cos(2\beta_e L) = -1. \tag{8}$$

So that the relation between β_e and *L* is given by,

$$\beta_e L = (2n+1)\,\pi/2. \tag{9}$$

From (6) and (9), the propagation constant of the two modes is thus obtained:

$$\frac{\beta_o}{\beta_e} = \frac{2n}{2n+1}. \tag{10}$$

When the difference between the propagation constants increases the coupled length *L* decreases. Therefore, smaller value of n corresponding to shorter coupler slot. Hence,

$$\beta_o/\beta_e = 2/3 \ (n=1). \tag{11}$$

In the coupling region of coupler, the propagation constant for $TE_{0.5,0}$ mode is given below:

$$\beta_e(f) = \sqrt{\left(\frac{2\pi\sqrt{\varepsilon_r}f}{c}\right)^2 - \left(\frac{\pi}{a_{eff}}\right)^2}. \tag{12}$$

According to the theory of Bethe hole, there is an approach to obtaining flat coupling versus frequency. So, the initial location of the coupling slot is given by [26], [27]:

$$D_{slot} = a_{eff}/4. \tag{13}$$

At the center frequency *f*, the initial length of the coupling region (*L*) may be determined by using formula (6), (10), (11), and (12).

C. EBG design

EBG structures are periodic structures that produce variations in the refractive index of the medium to introduce both a slow-wave effect and a certain stopband in its frequency response. The following step is to identify the EBG dimensions to be used for realizing out-of-band rejection. In Fig. 1 (b), there are five parameters to determine the band-gap properties: the periodic separation Lebg between adjacent EBG cells, the radius *r*1, the angle θ, the length lg, and the width *s1* of the GLS cell. The radius of the GLS structures *r1* (the first parameter) was increased in steps to find out its influence on the bandwidth and rejection, as shown in Fig. 4 (a).

The simulated results in Fig. 4 (a) revealed that for increasing radius of GLS, the relative bandwidth of the coupler was also found to decrease correspondingly. The parameters of the EBG cells (*r*1, *s*1) as well as the relative bandwidth are summarized in Table 1.

The second parameter is the width *s*1 of the EBG cell. Fig. 4 (b) shows the relationship between relative bandwidth and *s*1. The coupling bandwidth increases when the width *s*1 of the EBG cell is increased. In addition, smaller *s*1 corresponds to narrower bandwidth and steeper rolloff slope in transition band.

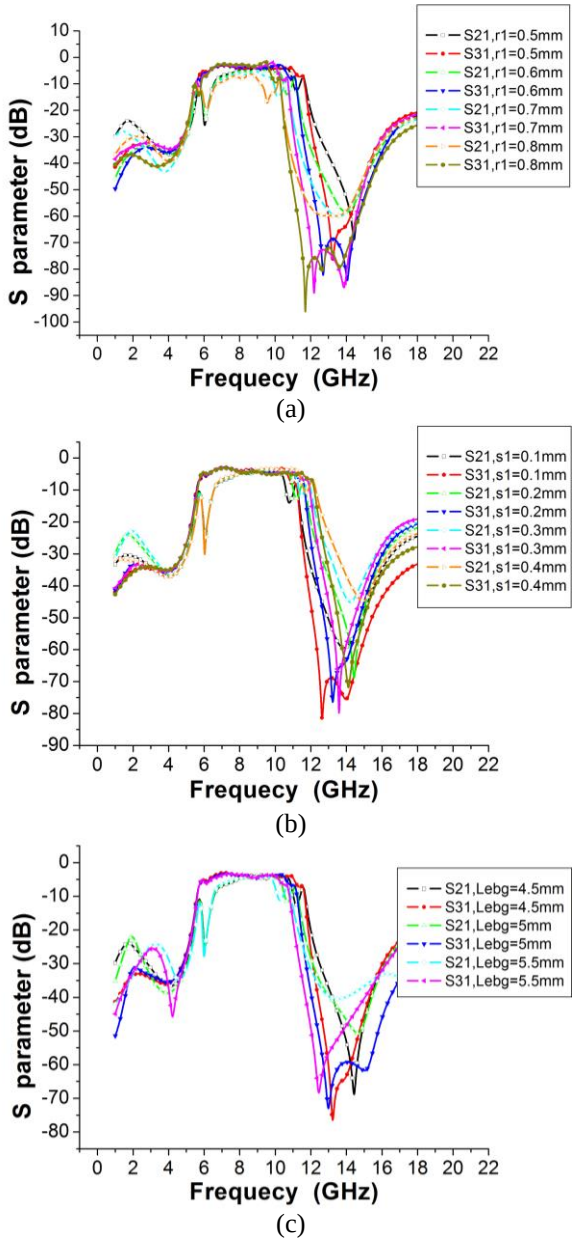

Fig. 4. Variation of frequency responses with respect to the parameters of the GLS cells: (a) the radius *r*1, (b) the width *s*1, and (c) the period Lebg.

Table 1: Relative bandwidth $\Delta f/f_0$ change with *r1* and *s*1

***r1* (mm)**	**$\Delta f/f_0$ (%)**	***s*1 (*mm*)**	**$\Delta f/f_0$ (%)**
0.5	38.16	0.1	34.18
0.6	33.42	0.2	38.16
0.7	27.44	0.3	42.04
0.8	23.16	0.4	45.19

The third parameter is the period Lebg of the structure, as it controls the center frequency of the stopband where Lebg=$\lambda_{gs}/2$ and λ_{gs} is the corresponding guided wavelength of the stopband center frequency. Lebg should be chosen such that, this stopband comes after the band of operation required.

The period (Lebg) of the EBG cells can be calculated by using HFSS. As shown in Fig. 4 (c), the center frequency of the stopband (f_s) reduces evidently with the distance between the EBG cells increased. Table 2 illustrates the period Lebg may affect the center frequency of the stopband and the corresponding guided wavelength.

Table 2: f_s and relative bandwidth change with *L*ebg

***L*ebg (*mm*)**	**f_s (GHz)**	**$\Delta f/f_0$ (%)**
4.5	15.85	38.16
5	15.79	35.79
5.5	15.17	32.56

The number of EBG structure controls the rejection whereas the bandwidth is determined by the size (which is controlled by the radius and width) of the EBG structure. Such configuration can be employed efficiently where wide-band stopband rejection is desired. Finally, the rest of the dimensions are estimated using HFSS simulation tool.

D. Coupling slot

As depicted in Fig. 1, the coupling slot is located on the metal plane between substrate 1 and 2. Moreover, the long coupling slot has variable lengths (Lslot), widths (Wslot) and offsets (Dslot), and the design parameters control the mutual coupling between two parallel waveguides.

From the formula (5), (6), and (12) we can see that the coupling ratio depends on the lengths (Lslot=L) of coupling slot. For a 3-dB coupler, $\Delta\beta$ decreases with increasing lengths (Lslot) of coupling slot. In addition, Lslot is also related to the center frequency of the coupler.

Table 3: Coupling ratio and f_0 change with Dslot

Dslot (mm)	**f_0 (GHz)**	**Coupling Ratio (dB)**
2.5	7.6370	-4.8276
3	8.6437	-4.1445
3.5	8.9273	-4.0869
4	9.0407	-3.9610
4.5	9.0832	-3.9045

But for a 6-dB coupler ($\Delta\beta L=\pi/3$), the length (Lslot=L) of coupling slot is shorter than the corresponding length of a 3-dB coupler. The other two parameters of the coupling slot have effects on both the coupling ratio and the center frequency.

According to the Table 3, both coupling ratio and the center frequency (**f_0**) of the coupler increase when the offset (Dslot) is increased.

Table 4: Coupling ratio and f_0 change with Wslot

Wslot (mm)	f_0 (GHz)	Coupling Ratio (dB)
2	8.9862	-3.9778
2.5	9.0430	-3.9611
3	9.2131	-3.9956
3.5	9.2273	-3.9917
4	9.2982	-4.0039

The simulated results in Table 4 revealed that for increasing widths (Wslot) of coupling slot, the center frequency of the coupler was also found to increase correspondingly. However, the change of coupling ratio is just the opposite. Moreover, it has to be noted that among all of the parameters of the slots, the offset distance (Dslot) has a critical effect. This is due to its direct impact on the field within the coupling slot as it causes a rapid variation for small offsets and slow variations for larger ones.

E. Deign example

In our design, the center frequency and relative bandwidth of the filtering coupler are 9 GHz and 36%, respectively. The used substrate is Taconic RF35 with relative permittivity (ε_r) of 3.5 and height of 0.508 mm.

Based on our knowledge, HMSIW structure has high-pass characteristics and can be used to realize lower sideband response of coupler. In addition, periodic ginkgo leaf slots (GLS) determine the center frequency of the stopband and can be used to form upper sideband response. As such, bandpass response of the coupler can be easily realized by combining above two characteristics. After the parameters of GLS cells have been properly adjusted, better out-of-band rejection in wideband may be achieved at the same time.

Therefore, the first step is to decide the dimensions of HMSIW structure. According to our specification, the cutoff frequency for the $TE_{0.5,0}$ dominant mode in HMSIW is estimated to 6.3GHz. By using (1), the initial values of width of HMSIW (a_{Hsiw}) should be 6.5 mm. There are six EBG cells in our design, as shown in Fig. 1. So, the length of the HMSIW should be at least more than five times of period of EBG cells. As such, the initial length of HMSIW can be determined as: L_{Hsiw}=8 *L*ebg.

The second step is to determine the parameters of GLS cells. As above discussion, the period of the GLS cells controls the center frequency of the stopband (f_{s0}) which can be calculated by using HFSS. According to Fig. 4 (c), Table 2, and our specification, the value ranges for the center frequency of the stopband are from 15.17 to 16GHz. Thus, the value ranges for period of EBG cells *L*ebg are from 4.5 to 6 mm.

The bandwidth and rolloff slope in the transition band are also affected by the radius *r1* and the width *s1* of the GLS structures. According to Table 1 and the specifications, the value ranges for the radius *r1* are from 0.5 to 0.6mm. Similarly, as observed in Table 1, the value ranges for the width *s*1 are from 0.1 to 0.3mm.

The third step is to calculate the length and location of coupling slot in HMSIW coupler. According to (6), (11), (12), and (13), the initial length (*L*slot) and location (*D*slot) of coupling slot should be 17.75mm and 3.38mm, respectively. Based on above considerations, the final optimal dimensions of the proposed coupler can be easily determined.

III. SIMULATED AND MEASURED RESULTS

After optimization implemented by HFSS, the geometry parameters of the proposed coupler are listed in Table 5. The proposed coupler was designed and fabricated on a substrate with thickness of 0.508 mm, relative dielectric constant of 3.5 and dielectric loss tangent 0.0018 (at 10 GHz). The simulated and measured results of S11, S21, S31 and S41 are presented in Fig. 5 (a).

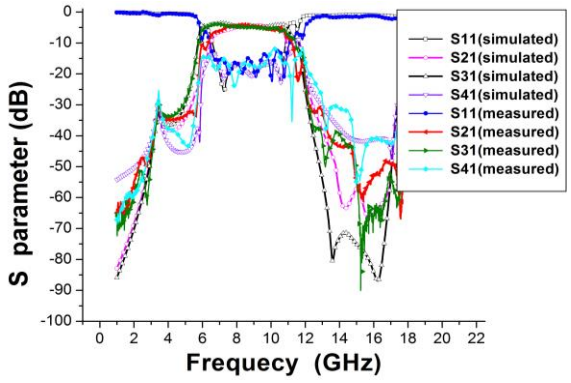

(a)

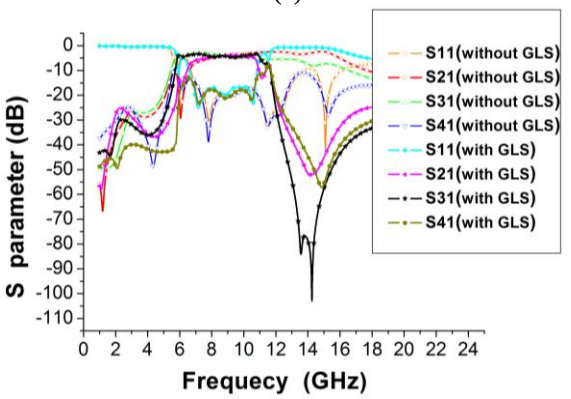

(b)

Fig. 5. Response of the coupler: (a) The proposed coupler with high selectivity, and (b) The coupler with and without GLS.

In the frequency range 6.6-10.7 GHz, the return loss (S11) is below -14.5dB. The isolation (S41) is above 15 dB in the range 6.1-10.5 GHz. With the acceptable

performance of S11 and S41, a measured power equality of -4.15±0.5 dB for S21 and S31 is achieved in the frequency range of 7.3-10.4GHz.

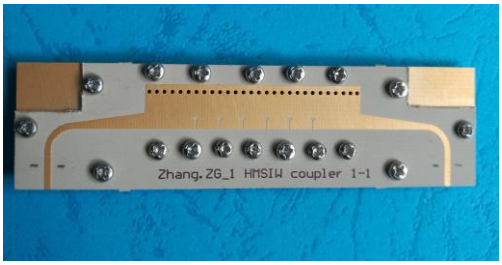

Fig. 6. Photograph of the fabricated coupler.

The insertion losses of the multilayer HMSIW filtering coupler are estimated to be nearly 1 dB in the frequency range 7.3-10.4 GHz. Its stop band is from 13.8 to 17.6GHz (Upper Sideband) with the rejection (S31) more than 40dB. In lower sideband (from 1 to 4.8GHz) the rejection is more than 25dB.

Table 5: Parameters of the fabricated coupler

***D* (mm)**	0.8	*W*strip (mm)	1.18
***p* (mm)**	1.5	Lstrip (mm)	11
ε_r	3.5	*W*siwH (mm)	6.5
***r1* (mm)**	0.5	*W*slot (mm)	2
***s1* (mm)**	0.2	*L*slot (mm)	16
θ (deg)	90	*D*slot (mm)	4
***L*ebg (mm)**	5	*lg* (mm)	3
LtaperH (mm)	13	*h* (mm)	0.508
WtaperH (mm)	3		

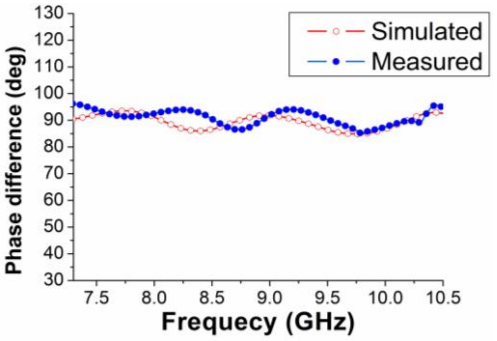

Fig. 7. Phase difference between Port 2 and Port 3.

As shown in Fig. 5 (b), the proposed coupler with GLS can realize high selectivity and improved coupling bandwidth. Compared with the coupler without GLS, the frequency selectivity and stopband suppression bandwidth of the proposed structure are improved evidently. In addition, the roll-off at the upper side is very sharper. The power equality points increased indicate that the coupling efficiency of the coupler is also improved. Figure 6 is the photograph of the fabricated HMSIW filtering coupler. The simulated phase difference is 90°±5° from 7.3 to 10.4GHz, as shown in Fig. 7.

Table 6: Performance comparison of SIW/HMSIW couplers

Ref.	**f_0 (GHz)/ FBW (%)**	**Size (λ_g^2)/ Isolation (dB)/ SFBW* (%)**	**Stopband Rejection (dB)/ Layers*/ε_r**
[2]	13/20	2.36/16/2.4	7/1/2.2
[5]	7/7	2.64/15/10.5	10/1/2.2
[12]	7.75/2.58	2.23/30/15.05	25/2/3.5
[14]	8/12.5	2.2/20/2.8	8/2/2.94
[15]	10.2/24.6	5.96/15/4	10/1/2.2
[16]	14.1/ 42	2.1/15/5.1	8/1/9.5
[28]	10.25/34	5.26/15/3.1	8/1/9.5
This work	8.87/34.9	2.2/15/24.64	40/2/3.5

Where λg is the guided wavelength on the substrate at the center frequency f_0, FBW represent the fractional bandwidth. Layers represent number of substrate layers. SFBW* represent the Stopband (Upper Sideband) fractional bandwidth.

A detailed performance comparison with SIW/ HMSIW couplers in recent years is shown in Table 6, which demonstrates the advantage of the proposed coupler clearly. Compared with the works in Table 6, the proposed structure has the better stop-band rejection and steeper transition band.

Its stop band is from 13.8 to 17.6GHz with the rejection more than 40dB. The stopband (Upper Sideband) fractional bandwidth is about 24.64%. Compared with the works in [2], [5], [12], [14], and [15], the presented coupler has featured wider bandwidths and lower loss.

IV. CONCLUSION

A novel multilayer 3dB filtering coupler with high selectivity has been proposed and developed in multilayer HMSIW topology. This modification allows HMSIW operation, resulting in significant size reduction using both multilayer and half-mode schemes simultaneously. Moreover, the novel GLS cells are etched on top layer of HMSIW to realize filtering coupler, which is a kind of multifunctional structure. Since the proposed structure integrates a bandpass filter and a directional coupler, it can contribute to the miniaturization of an RF transceiver. Compared with the coupler without GLS, the frequency selectivity and stopband suppression bandwidth of the proposed structure are improved evidently. It's a good combination of multilayered topologies, HMSIW and EBG structures. The proposed wideband coupler with GLS shows advantages of low cost, compact size, high selectivity and wide stopband

bandwidth, indicating it being a good candidate for wideband wireless communication applications.

ACKNOWLEDGMENT

This work was supported in part by the Ministry of Science and Technology of the People's Republic of China under grant 2013YQ200503 and in part by the National Natural Science Foundation of China (NSFC) under grant 61001028.

REFERENCES

[1] W. Hong, B. Liu, et al., "Integrated microwave and millimeter wave antennas based on SIW and HMSIW technology," *IEEE International Workshop on Antenna Technology (iWAT'2007*), Cambridge, UK, pp. 69-72, Mar. 2007.

[2] B. Liu, W. Hong, Y. Q. Wang, Q. H. Lai, and K. Wu, "Half mode substrate integrated waveguide (HMSIW) 3dB coupler," *IEEE Microw. Wireless Compon. Lett.*, vol. 17, no. 1, pp. 22-24, Jan. 2007.

[3] Y. J. Cheng, W. Hong, K. Wu, and Y. Fan, "A hybrid guided-wave structure of half mode substrate integrated waveguide and conductor-backed slotline and its application in directional couplers," *IEEE Microw. Wireless Compon. Lett*., vol. 21, no. 2, pp. 65-67, Feb. 2011.

[4] M. H. Ho and C. S. Li, "Novel balanced bandpass filters using substrate integrated half-mode waveguide," *IEEE Microw. Wireless Compon. Lett.*, vol. 23, no. 2, pp. 78-80, Feb. 2013.

[5] R. J. Thomas and M. Daneshmand, "The characterization of a ridged Half-Mode Substrate-Integrated Waveguide and its application in coupler design," *IEEE Trans. Microw. Theory Tech*., vol. 64, no. 11, pp. 3580-3591, Apr. 2016.

[6] W. Shao and J. L. Li, "Design of a half-mode SIW high-pass filter," *Appl. Comp. Electro. Society (ACES) Journal*, vol. 26, no. 5, pp. 447-451, May 2011.

[7] G. H. Zhai, W. Hong, K. Wu, J. X. Chen, P. Chen, and H. J. Tang, "Substrate integrated folded waveguide (SIFW) narrow-wall directional coupler," *International Conference on Microwave and Millimeter Wave Technology*, Nanjing, China, vol. 1, pp. 174-177, Apr. 2008.

[8] P. L. Chi and T. Y. Chen, "Dual-band ring coupler based on the composite right/left-handed folded substrate integrated waveguide," *IEEE Microwave and Wireless Components Letters*, vol. 24, no. 5, pp. 330-332, May 2014.

[9] J. R. Aitken, J. S. Hong, and Z. C. Hao, "Out-of-phase power divider based on two-layer SIW," *Electron Lett*., vol. 50, no. 14, pp. 1005-1007, July 2014.

[10] C. Wang, W. Q. Che, and P. Russer, "High-isolation multiway power dividing/combining network implemented by broadside-coupling SIW directional couplers," *International Journal of RF and Microwave Computer-Aided Engineering*, vol. 19, no. 5, pp. 577-582, Sep. 2009.

[11] Z.-G. Zhang, Y. Fan, and Y.-H. Zhang, "Compact 3-D multilayer substrate integrated circular and elliptic cavities (SICCs and SIECs) dual-mode filter with high selectivity," *Appl. Comp. Electro. Society (ACES) Journal*, vol. 28, no. 4, pp. 333-340, Apr. 2013.

[12] Y. J. Cheng and Y. Fan, "Compact substrate-integrated waveguide bandpass rat-race coupler and its microwave applications," *IET Microwaves, Antennas & Propagation*, vol. 6, no. 9, pp. 1000-1006, June 2012.

[13] O. A. Nova, J. C. Bohórquez, N. M. Peña, G. E. Bridges, L. Shafai, and C. Shafai, "Filter-antenna module using substrate integrated waveguide cavities," *IEEE Microw. Wireless Compon. Lett*., vol. 10, no. 1, pp. 59-62, June 2011.

[14] A. A. M. Ali, H. B. El-Shaarawy, and H. Aubert, "Miniaturized hybrid ring coupler using electromagnetic bandgap loaded ridge substrate integrated waveguide," *IEEE Microw. Wireless Compon. Lett.*, vol. 21, no. 9, pp. 471-473, Sep. 2011.

[15] X. Zou, C. M. Tong, C. Z. Li, and W. J. Pang, "Wideband hybrid ring coupler based on Half-Mode Substrate Integrated Waveguide," *IEEE Microwave and Wireless Components Letters*, vol. 24, no. 9, pp. 596-598, Sep. 2014.

[16] H. Y. Jin, Y. L. Zhou, Y. M. Huang, S. Ding, and K. Wu, "Miniaturized broadband coupler made of slow-wave half-Mode substrate integrated waveguide," *IEEE Microw. Wireless Compon. Lett.*, vol. 27, no. 2, pp. 132-134, Feb. 2017.

[17] R. Rezaiesarlak, M. Salehi, and E. Mehrshahi, "Hybrid of moment method and mode matching technique for full-wave analysis of SIW circuits," *Appl. Comp. Electro. Society (ACES) Journal*, vol. 26, no. 8, pp. 688-695, Aug. 2011.

[18] I. Bouchachi, J. Mateu, and M. L. Riabi, "Waveguide filter modeling and dimulation using mode-matching, fullwave network analysis and swarm optimization," *Appl. Comp. Electro. Society (ACES) Journal*, vol. 32, no. 2, pp. 169-177, Feb. 2017.

[19] Z. J. Zhu, L. Cao, and C. L. Wei, "Novel compact microstrip dual-Mode filters with two controllable transmission zeros," *Appl. Comp. Electro. Society (ACES) Journal*, vol. 33, no. 1, pp. 43-48, Jan. 2018.

[20] L. X. Zhou, S. J. Liu, J. Duan, and M. Xun, "A novel tunable combline bandpass filter based on external quality factor and internal coupling tunings," *Appl. Comp. Electro. Society (ACES) Journal*, vol. 33, no. 6, pp. 690-696, June 2018.

[21] Y. S. Li, W. X. Li, W. H. Yu, and C. Y. Liu, "A miniaturization band-pass filter with ultra-narrow multi-notch-band characteristic for ultra-wideband communication applications," *Appl. Comp. Electro. Society (ACES) Journal*, vol. 29, no. 4, pp. 289-300, Apr. 2014.

[22] W. J. Feng, M. L Hong, and W. Q. Che, "Narrow-band bandpass filters with improved upper stop-band using open/shorted coupled lines," *Appl. Comp. Electro. Society (ACES) Journal*, vol. 31, no. 2, pp. 152-158, Feb. 2016.

[23] L. X. Zhou, Y. Z. Yin, W. Hu, and X. Yang, "Compact bandpass filter with sharp out-of-band rejection and its application," *Appl. Comp. Electro. Society (ACES) Journal*, vol. 32, no. 3, pp. 249-255, Mar. 2017.

[24] Y. Li, W. Li, C. Liu, and Q. B. Ye, "A compact UWB band-pass filter with ultra-narrow tri-notch-band characteristic," *Appl. Comp. Electro. Society (ACES) Journal*, vol. 29, no. 2, pp. 170-177, Feb. 2014.

[25] S. I. Yamamoto, J. Hirokawa, and M. Ando, "Length reduction of a short-slot directional coupler in a single-layer dielectric substrate waveguide by removing dielectric near the side walls of the coupler," *IEEE Antennas and Propagation Society International Symposium*, Monterey, CA, vol. 8, pp. 2353-2456, June 2004.

[26] R. Levy, "Analysis and synthesis of waveguide multi-aperture directional couplers," *IEEE Trans. Microw. Theory Tech.*, vol. 16, no. 12, pp. 995-1006, Apr. 1968.

[27] A. A. Oliner, "Equivalent circuits for small symmetrical longitudinal apertures and obstacles," *IRE Trans. Microw. Theory Tech.*, vol. 8, no. 12, pp. 72-80, Jan. 1960.

[28] H. Jin, L. Jian, and G. Wen, "A novel coupler based on HMSIW," *IEICE Trans. Electron.*, vol. E93-C, no. 2, pp. 205-207, Feb. 2010.

Zhigang Zhang was born in Shanxi Province, China. He received the B.S. degree in Electronic Information Engineering and M.S. degree in Wireless Physics from Sichuan University and is currently working toward the Ph.D. degree in Electromagnetic Field and Microwave Technology from The University of Electronic Science and Technology of China (UESTC), Chengdu, Sichuan, China. His current research interests include SIW technology and its application, microwave and millimeter-wave filters, and couplers, electromagnetic theory.

Yong Fan received the B.E. degree from the Nanjing University of Science and Technology, Nanjing, Jiangsu, China, in 1985, and the M.S. degree from the University of Electronic Science and Technology of China (UESTC), Chengdu, Sichuan, China, in 1992.

He is currently with the School of Electronic Engineering, UESTC. He has authored or coauthored over 60 papers. From 1985 to 1989, he was interested in microwave integrated circuits. Since 1989, his research interests include millimeter-wave communication, electromagnetic theory, millimeter-wave technology, and millimeter-wave systems. Mr. Fan is a Senior Member of the Chinese Institute of Electronics (CIE).

Yonghong Zhang received the B.S., M.S., and Ph.D. degrees from the University of Electronic Science and Technology of China (UESTC), Chengdu, China, in 1992, 1995, and 2001, respectively. From 1995 to 2002, he was a Teacher with the UESTC. In 2002, he joined the Electronic Engineering Department, Tsinghua University, Beijing, China, as a Doctoral Fellow. In 2004, he rejoined the UESTC. His research interests are in the area of microwave and millimeter-wave technology and applications.